SUPPORTING INFORMATION: RECONSTITUTION OF HELICAL SOLUBLE α-SYNUCLEIN THROUGH TRANSIENT INTERACTION WITH LIPID INTERFACES

Matteo Rovere[a], John B. Sanderson[a], Luis Fonseca-Ornelas[a], and Tim Bartels[a]

[a]Ann Romney Center for Neurologic Diseases, Brigham and Women's Hospital and Harvard Medical School, 60 Fenwood Road, 02115-6128 Boston, MA, United States

CORRESPONDING AUTHOR:
Tim Bartels
Ann Romney Center for Neurologic Diseases
60 Fenwood Road
BTM 10002N
Boston, MA 02115-6128
Phone: +1-617-525-5271
E-mail: tbartels@rics.bwh.harvard.edu

SI Materials and Methods

Materials. 1,2-didodecanoyl-*sn*-glycero-3-phosphocholine (12:0 PC or DLPC), 1,2-ditridecanoyl-*sn*-glycero-3-phosphocholine (13:0 PC), 1,2-dimyristoyl-*sn*-glycero-3-phosphocholine (14:0 PC or DMPC) and 1,2-dipentadecanoyl-*sn*-glycero-3-phosphocholine (15:0 PC) were purchased from Avanti Polar Lipids (Alabaster, AL) as dry powder. All other chemicals were obtained from Sigma-Aldrich (St. Louis, MO) unless otherwise noted.

Protein Expression and Purification. A construct based on the sequence of human α-synuclein (αSyn) in pET5a was used to transform BL21(DE3) *E.coli*. The bacteria were co-transformed with a pACYCDuet-1 plasmid containing cDNA encoding for both the catalytic (Naa20) and regulatory (Naa25) subunits of the fission yeast NatB complex (pNatB) (1), a generous gift from Daniel P. Mulvihill (University of Kent, UK). Bacterial cultures were induced at an OD_{600} of 0.5 with 1 mM isopropyl-β-D-thiogalactopyranoside (IPTG) for 4 hrs. The cell pellet, after harvesting, was resuspended in 20 mM Tris buffer, 25 mM NaCl, pH 8.00, and lysed by boiling for 15 min. The supernatant of a 20 min., 20,000xg spin of the lysate was then further processed. The sample was loaded on two 5-mL (tandem) HiTrap Q HP anion exchange columns (GE Healthcare, Pittsburgh PA), equilibrated with 20 mM Tris buffer, 25 mM NaCl, pH 8.00. αSyn was eluted from the columns with a 25-1000 mM NaCl gradient in 20 mM Tris buffer, 1 M NaCl, pH 8.00. Peak fractions were pooled and injected on two 5-mL (tandem) HiTrap Phenyl HP hydrophobic interaction columns (GE Healthcare, Pittsburgh, PA), equilibrated with 50 mM phosphate buffer, 1 M $(NH_4)SO_4$, pH 7.40. αSyn was eluted from the columns with a 1000-0 mM $(NH_4)SO_4$ gradient in Milli-Q water. Peak fractions from the two peaks (N-alpha-acetylated and non-N-alpha-acetylated αSyn) were further purified via gel filtration on a Superdex 200 XK 26/100 column (GE Healthcare, Pittsburgh, PA) using 50 mM $(NH_4)Ac$, pH 7.40 as running buffer. The peak fractions were lyophilized and N-terminal acetylation was validated by intact mass spectrometry. Lyophilized protein was kept at 4ºC and reconstituted fresh, before experiments, in 10 mM $(NH_4)Ac$, pH 7.40. The solution was also spun down every time after resuspension, before spectroscopic quantitation of the protein concentration, at 21,130xg for 20 min. at 4ºC to remove any large αSyn aggregates. Concentration was evaluated measuring the absorbance at 280 nm (ε=0.412 $mg \cdot mL^{-1} \cdot cm^{-1}$).

SUVs Preparation. Lipid solutions were prepared fresh by resuspending the lyophilized lipids in 10 mM $(NH_4)Ac$, pH 7.40 to their final concentrations and hydrating them for 30 min. in a water bath, at a temperature higher than their T_m. SUVs were prepared by pulse-sonicating the phospholipid suspensions for 10-20 min. at RT with a microtip sonicator (Misonix S-4000, Qsonica, Newtown, CT). The vesicle suspensions were spun down at 21,130xg for 10 min. to remove any metal particles and larger lipid aggregates.

CD. Spectra and temperature scans were recorded with a Jasco 810 spectropolarimeter (Jasco, Easton, MD). When possible, buffer-only or lipid blank spectra, obtained by measuring the scattering profile of the SUVs suspension alone in buffer, were recorded and subtracted. Temperature control with an accuracy of ±0.1ºC in the cuvette was achieved with a heating/cooling accessory equipped with a Peltier element (PFD-425S) connected to a water thermostatic bath. Before taking the numerical first derivative, the 222-nm ellipticity signal was smoothed twice using a Savitzky-Golay filter.

ITC. Isothermal titration calorimetry measurements were performed with an iTC200 instrument (Malvern Instruments, Westborough, MA). Typically, 18 fresh SUVs dispersion injections of 2 µL each (+1 0.4 µl pre-injection) were titrated in the calorimeter chamber containing 204 µL of the protein solution. Both

linear baselines and control titrations of vesicles into buffer alone were used for baseline subtraction. The data were processed using the MicroCal ORIGIN 7.0 software. After integration of the differential heat signal, stoichiometric and thermodynamic parameters (*N, ∆H, K*) were determined fitting the sigmoidal titration curve using a model that assumes the existence of *N* independent identical saturable protein binding sites on the outer surface of the vesicles. The apparent binding constant, given the approximations used, was labeled K_{app}. The total lipid concentration in the syringe was taken as the ligand concentration. The aggregation state of the lipids and the accessibility of the inner lipid bilayer of the vesicles were neglected. Fitted parameters are reported with their standard errors from the fitting. ΔS was obtained from $\Delta G = -RTlnK_{app}$ and ΔH.

DSC. Differential scanning calorimetry was performed with a VP-DSC instrument (Malvern Instruments, Westborough, MA). SUVs suspensions were prepared fresh before the experiments and all solutions were degassed before use. Scans were recorded between 50ºC and 5ºC at a rate of 30ºC/hr. and under an instrument-controlled positive pressure of approximately 30 p.s.i. Linear baselines were subtracted using the MicroCal ORIGIN 7.0 software.

DLS. The hydrodynamic radius of the liposomes was assessed using a DynaPro dynamic light scattering instrument (Wyatt Technology Corporation, Santa Barbara, CA). The DLS cell was thermostated at 25.0ºC; the hydrodynamic radii of the samples were obtained from the averages of 30 recordings of the same sample.

NMR. ^{1}H-NMR spectra of 10 μM αSyn, either in the presence or in the absence of freshly prepared 12 mM 13:0 PC SUVs, were recorded in 10 mM (NH_4)Ac, pH 7.40, 10% D_2O, at different temperatures. Spectra were recorded on a 600MHz Bruker AVANCE II spectrometer (Bruker, Billerica, MA). Control over the gradient during the temperature cycling step of the refolding protocol was manually achieved through the thermostating element of the probe and the cycling was performed between 50ºC and 10ºC at 0.5ºC/min. Data processing and analysis were perfomed with the Bruker TopSpin software.

EM. EM specimens were prepared on carbon-coated grids rendered hydrophilic by glow discharge. Samples, freshly prepared, were adsorbed on the grids with a 30-sec. incubation. For negatively-stained samples, the grids were stained with 1% (w/v) aqueous uranyl acetate for 2 min. For immunogold-labeled samples, after sample adsorption on the grids, the grids were blocked with 1% bovine serum albumin (BSA) for 10', then incubated with primary antibody (15G7) in 1% BSA for 30 min., washed (3x) for 10 min. in PBS, then incubated with a rabbit-anti-rat bridging antibody in 1% BSA for 20 min. After 3 more washes in PBS (10 min.), the grids were incubated in Protein A-gold (5 nm) in 1% BSA for 20 min., then washed in PBS (2x, 5 min.) and water (4x, 10 min.) and negatively stained with 1% (w/v) aqueous phosphotungstic acid (PTA) for 2 min. Imaging was performed on a JEOL 1200EX transmission electron microscope (JEOL USA Inc., Peabody, MA) and images were recorded with an AMT 2k CCD camera. The number of immunogold particles (either on or off the SUVs' membranes) and the number of SUVs were manually quantified from 10 micrographic fields obtained from 3 independent experiments.

αSyn cell lines and transfection. All materials were purchased from Invitrogen (Thermo Fisher Scientific, Waltham, MA) unless stated otherwise. Cells were cultured at 37ºC in 5% CO_2. Human neuroblastoma cells (BE(2)-M17; ATCC number CRL-2267) were cultured in Dulbecco's modified Eagle's medium (M17D) (2) supplemented with 10% FBS, 100 units/ml penicillin, 100 μg/ml streptomycin and 2 mM L-glutamine. M17D cells were transfected using Lipofectamine 2000 according to the manufacturer's directions. The stable monoclonal cell line M17D/αSyn was generated by transfection of M17D cells with

pcDNA4-αSyn, followed by zeocin selection and isolation of single clones.

αSyn and intact-cell cross-linking. Cross-linking of intact M17D cells was performed as previously described (3). For recombinant αSyn cross-linking, DSG was prepared immediately before use at 10x final concentration in DMSO. Samples were incubated with cross-linker for 30 min. at RT. The reaction was quenched with the addition of 1 M Tris, pH 7.50, to 50 mM final concentration and incubated for 15 min. at RT.

Antibodies. 2F12 and SOY1 monoclonal mouse antibodies against human αSyn (Cat. No. MABN1817 for 2F12, MABN1818 for SOY1) were obtained from Sigma-Aldrich (St. Louis, MO). The 15G7 monoclonal rat antibody against human αSyn (Cat. No. ALX-804-258-LC05) was obtained from Enzo Life Sciences (Farmingdale, NY).

Immunoblotting. Electrophoresis and blotting reagents were obtained from Thermo Fisher Scientific (Waltham, MA) unless otherwise noted. Samples were prepared for electrophoresis by the addition of 4x NuPAGE LDS sample buffer. Samples were electrophoresed on NuPAGE Novex 4-12% Bis-Tris gels with NuPAGE MES-SDS running buffer and using the SeeBlue Plus2 MW marker. After electrophoresis, gels were electroblotted onto Immobilon-PSQ 0.2 µm PVDF membrane (Millipore, Billerica, MA) for 1 hr. at 400 mA constant current at 4ºC in 25 mM Tris, 192 mM glycine, 20% (v/v) methanol transfer buffer. After transfer, the membranes of gels run with lysate samples were incubated in 4% (m/v) paraformaldehyde in phosphate buffered saline (PBS) for 30 min. at RT, rinsed (3x) 5 min. with PBS and blocked with a 5% milk solution (PBS containing 0.1% (v/v) Tween 20 (PBS-T) and 5% (m/v) powdered milk) for either 1 hr. at RT or overnight at 4ºC. After blocking, membranes were incubated in primary antibody in 5% milk solution for either 1 hr. at RT or overnight at 4ºC. Membranes were washed (3x) 5 min. in PBS-T at RT and incubated (30 min. at RT) in horseradish peroxidase-conjugated secondary antibody (GE Healthcare, Pittsburgh, PA) diluted 1:10,000 in 5% milk solution. Membranes were then washed (3x) 5 min. in PBS-T and developed with SuperSignal West Dura according to manufacturers' instructions. 2F12 was used at 0.18 µg/mL.

SEC. Samples were injected on a Superdex 200 (10/300 GL) column (GE Healthcare, Pittsburgh, PA) at RT and eluted with 50 mM (NH_4)Ac, pH 7.40. For size estimation, a gel filtration standard (Catalog #151-1901, Bio-Rad, Hercules, CA) was run on the column, and the calibration curve was obtained by semi-logarithmic plotting of molecular weight versus the elution volume divided by the void volume.

ELISA. All materials were purchased from MSD (Meso Scale Discovery, Rockville, MD) unless stated otherwise. For αSyn ELISAs, 96-well Multi-Array Standard Bind plates were coated with the capture antibody 2F12 diluted (6.7 ng/µl) in phosphate-buffered saline (PBS) in 30 µl/well and incubated at 4ºC overnight. After emptying the wells, plates were blocked for 1 hr. at RT in blocking buffer (5% (m/v) MSD Blocker A in tris-buffered saline with 0.05% Tween 20 (v/v) (TBS-T)). After 5 washes with TBS-T, samples, diluted in TBS-T with 1% (m/v) MSD Blocker A and 0.5% (v/v) NP40, were loaded and incubated at 4ºC overnight. Sulfo-tagged SOY1 (detection antibody) was generated using Sulfo-Tag-NHS-Ester, diluted in blocking buffer (6.7 ng/µl), added to the plate (30 µl/well) and shaken for 1 hr. at RT. After 5 TBS-T washes, MSD Read Buffer diluted 1:1 in ultrapure water was added and the plates were immediately measured using a MSD Sector 2400 imager. The Lower Limit of Quantification (LLOQ) was set at the signal from the blank plus 9 times the Standard Deviation from duplicate wells.

Quantitative phosphate analysis. The protocol used is adapted from Chen *et al*. (4). Samples were

transferred to the bottom of glass test tubes, 22.5 µl of ~8.90 N H_2SO_4 were added, and the mixture was heated for 25 min. at 200-215ºC. Next, 7.5 µl of 30% (v/v) H_2O_2 were added to all of the tubes, after cooling them down to RT. After heating the samples again for 30 min. at 200-215ºC and cooling them down to RT, 195 µl of Milli-Q water and then 25 µl of a 2.5% (m/v) ammonium molybdate (VI) tetrahydrate solution were added. After addition of 25 µl 10% (m/v) ascorbic acid solution, the tubes were heated for 7 min. at 100ºC, and samples were cooled down again to RT. Absorbance at 820 nm was measured and phosphate concentration calculated using a calibration curve obtained from 5 phosphate samples ranging from 10 to 100 nmol, prepared from a 1000 mg/L phosphate standard solution for IC.

Data analysis and kinetic modelling. Global curve fitting for the unfolding data was performed using GraphPad Prism 6 applying a biphasic model with all parameters constrained among the curves except for $LogEC_{50,2}$ and $n_{H,2}$ (See Fig. S7 for details). The final plateau value was set at 0 for all curves. The systems of kinetic differential equations were solved (either analytically or numerically) and plotted using Wolfram Mathematica 10 (see SI Appendix for details).

SI Appendix
Kinetic analysis of the unfolding of αSyn

In order to dissect the binding and unfolding kinetics of αSyn in the presence of lipid interfaces, three mechanistic hypotheses were designed, corresponding to three different mechanisms of αSyn-lipid and αSyn-αSyn interaction. These models were described with differential equations, then solved (either analytically or numerically) and plotted in order to compare their time course with the data measured from the CD-followed unfolding kinetics. It must be noted that the ellipticity signal at 222 nm, after being converted to a percentage value of the maximum helicity (0 hrs), can be used to monitor the unfolding kinetics, but it is the combined value of both the folded and bound species and the folded, unbound αSyn. All the binding and unbinding processes were modeled as elementary reaction steps with a reaction order equal to the number of species involved. SUV-αSyn is a binding site for αSyn on the vesicle surface occupied by αSyn; SUV is a free binding site; αSyn is folded, unbound, αSyn; αSyn' is unfolded, unbound αSyn.

Mechanistic Hp. A

The first hypothesis tested was the possibility that αSyn was still bound to the vesicles and that any folded species unbound from the interfaces were short-lived intermediates that would rapidly unfold. The slow unfolding would have then reflected the slow, irreversible, unbinding of αSyn caused by the hysteresis in the lipid-binding equilibrium, not in the conformation of the protein.

$$[\text{SUV-}\alpha\text{Syn}] \overset{k_1}{\rightarrow} [\text{SUV}] + [\alpha\text{Syn}] \overset{k_2}{\rightarrow} [\alpha\text{Syn}']$$

$$\begin{cases} \dfrac{\mathrm{d}[\text{SUV-}\alpha\text{Syn}]}{\mathrm{d}t} = -k_1[\text{SUV-}\alpha\text{Syn}] \\ \dfrac{\mathrm{d}[\alpha\text{Syn}]}{\mathrm{d}t} = k_1[\text{SUV-}\alpha\text{Syn}] - k_2[\alpha\text{Syn}] \\ \dfrac{\mathrm{d}[\alpha\text{Syn}']}{\mathrm{d}t} = k_2[\alpha\text{Syn}] \end{cases}$$

The boundary conditions are *[SUV-αSyn](0) = c_0*, *[αSyn](0) = [αSyn'](0) = 0*. This system of ordinary differential equations (ODEs) has an analytical solution. To solve the system, one can start from the first equation, separating the variables, and then substitute the solution (an exponential decay) in the second equation. The second ODE is now a nonhomogeneous linear first-order differential equation and can be solved using the method of undetermined coefficients. The third equation can either be solved by integration of *[αSyn](t)* or by simply using the fact that the sum of the three species is c_0. In order to account for the dilution, a dilution factor *w* can be introduced in the system, multiplying every concentration. In this first system of ODEs, though, all the *w*s cancel out (in accord with the fact that, intuitively, with such a mechanism, there should be no dependence on concentration). The only *w* remaining is in the boundary condition for *[SUV-αSyn](0)*: *[SUV-αSyn](0) = $w \cdot c_0$*, which accounts for the reduction of the total signal by a *w* factor (the experimental data were renormalized accordingly to help the comparison of the different curves). The solutions thus are:

$$\begin{cases} [\text{SUV-}\alpha\text{Syn}] = wc_0 \cdot \mathrm{e}^{-k_1 t} \\ [\alpha\text{Syn}] = wc_0 \cdot \dfrac{k_1 \mathrm{e}^{(-k_1 t - k_2 t)}(-\mathrm{e}^{k_1 t} + \mathrm{e}^{k_2 t})}{k_1 - k_2} \\ [\alpha\text{Syn}'] = wc_0 \cdot \dfrac{\mathrm{e}^{(-k_1 t - k_2 t)}(-k_1 \mathrm{e}^{k_1 t} + k_1 \mathrm{e}^{(k_1 t + k_2 t)} + k_2 \mathrm{e}^{k_2 t} - k_2 \mathrm{e}^{k_1 t + k_2 t})}{k_1 - k_2} \end{cases}$$

Even before plotting these solutions, the functional form of the equations alone shows no dependency (other than the starting value) from the dilution factor *w*; it follows that the shape of the curves for the three dilution factors at which the kinetics were measured (*w* = 1, 0.5, 0.25) will be exactly the same. Plots of the curves (*[SUV-αSyn]+[αSyn]*) for k_1 = 0.15, k_2 = 0.7, c_0 = 100 and *w* = 1, 0.5, 0.25 (respectively blue, red and green) confirm this (the curves were plotted with these parameters and then rescaled by a factor w^{-1} to account for dilution, as was done with the experimental data). The three curves overlay perfectly and hence only the curve for *w* = 1 is visible:

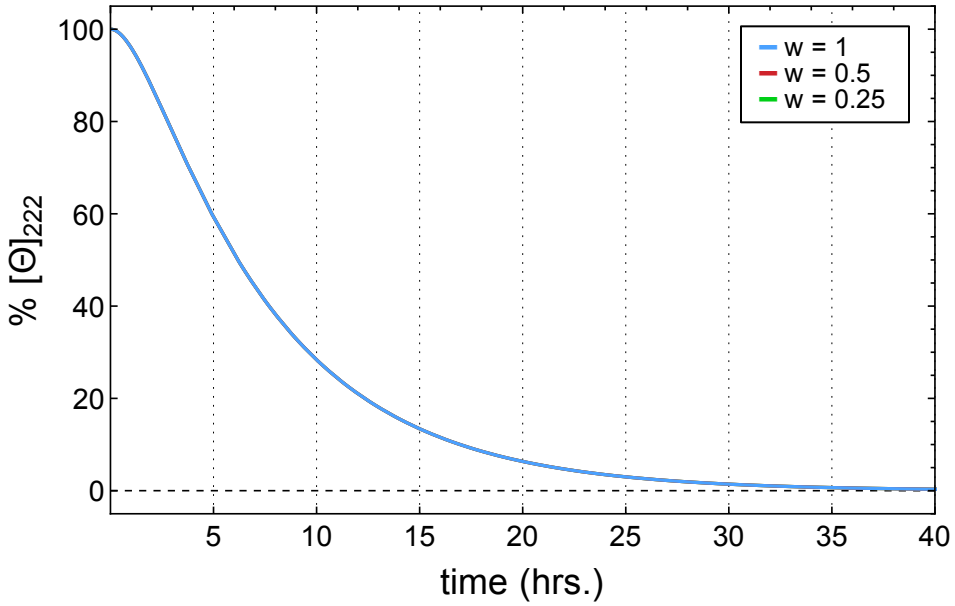

The kinetic equations obtained from this mechanistic hypothesis cannot reproduce the concentration dependence and the biphasic shape of the observed unfolding curves (Fig. 5B). We can therefore conclude that the slow unfolding of αSyn cannot be explained by a concomitant unbinding process from the membranes.

Mechanistic Hp. B

Given the peculiar shape of the kinetic curves at *w* = 0.5 and 0.25, we accounted for the presence of a biphasic process modifying our equations with a sigmoidal term, a classic functional form widely used in the description of cooperative processes (5). Sigmoidal kinetic curves are also typical of autocatalytic reactions (6). In this case, the autocatalysis can be mechanistically interpreted with a weak, dynamic,

multimerization process of the folded species (which would be in agreement with previous work (3,7) and would also be consistent with the band pattern observed in Fig. S6) increasing the lifetime of the folded monomers. The choice of where to insert this term in the system of ODEs (and thus in the mechanism) was grounded in a number of observations about the behavior of αSyn and also based on the body of experimental data collected in our work. A cooperative behavior leading to the concerted unfolding of αSyn from the lipid-bound state, as in *[SUV-αSyn] → [SUV][αSyn']* would not have been able to justify the overwhelming majority of unbound αSyn at t = 0 hrs, as quantified by two independent techniques, nor it could account for the fact that the kinetic observed is multimolecular (concentration-dependent). If most of the αSyn is unbound at t = 0 hrs, without postulating a reverse lipid-binding process (that we are not assuming in this mechanism), this event could not be a major component of the kinetic, especially at later times, when it should become predominant (while initially the three samples have very similar unfolding curves). Analogously, a cooperative unbinding of αSyn (*[SUV-αSyn] → [SUV][αSyn]*) could have followed the observed time course only if the unbinding step were the rate-determining step of the reaction, thus defining the overall reaction rate and the shape of the kinetic curves. This assumption, though, clashes again with the evidence that most of the αSyn is unbound at t = 0 hrs; if this were the case, we would see kinetic curves decreasing steeply and with the same time constant, as the unbinding would just be a minor component, especially at later times. Thus, there is only one option available for the insertion of the sigmoidal term; it has to be between the second and third step of the kinetic: *[αSyn] → [αSyn']*. The unfolding constant k_2 can be unified with the new term and the second step of the kinetic can be described with a complex dependency of k_2 from both *[αSyn]* and w, which is how we have referred to it, for the sake of brevity, in the main text and in superscripts: $k_2(w,[\alpha\text{Syn}])$:

$$[\text{SUV-}\alpha\text{Syn}] \overset{k_1}{\rightarrow} [\text{SUV}] + [\alpha\text{Syn}] \overset{k_2(w,[\alpha\text{Syn}])}{\longrightarrow} [\alpha\text{Syn}']$$

$$\begin{cases} \dfrac{\mathrm{d}[\text{SUV-}\alpha\text{Syn}]}{\mathrm{d}t} = -k_1[\text{SUV-}\alpha\text{Syn}] \\ \dfrac{\mathrm{d}[\alpha\text{Syn}]}{\mathrm{d}t} = k_1[\text{SUV-}\alpha\text{Syn}] - k_2[\alpha\text{Syn}] - \dfrac{k_4[\alpha\text{Syn}]}{1+\mathrm{e}^{-\sigma([\alpha\text{Syn}]-c_t(w))}} \\ \dfrac{\mathrm{d}[\alpha\text{Syn}']}{\mathrm{d}t} = k_2[\alpha\text{Syn}] + \dfrac{k_4[\alpha\text{Syn}]}{1+\mathrm{e}^{-\sigma([\alpha\text{Syn}]-c_t(w))}} \end{cases}$$

or:

$$[\text{SUV-}\alpha\text{Syn}] \overset{k_1}{\rightarrow} [\text{SUV}] + [\alpha\text{Syn}] \overset{k_2(w,[\alpha\text{Syn}])}{\longrightarrow} [\alpha\text{Syn}']$$

$$\begin{cases} \dfrac{\mathrm{d}[\text{SUV-}\alpha\text{Syn}]}{\mathrm{d}t} = -k_1[\text{SUV-}\alpha\text{Syn}] \\ \dfrac{\mathrm{d}[\alpha\text{Syn}]}{\mathrm{d}t} = k_1[\text{SUV-}\alpha\text{Syn}] - k_2(w,[\alpha\text{Syn}])[\alpha\text{Syn}] \\ \dfrac{\mathrm{d}[\alpha\text{Syn}']}{\mathrm{d}t} = k_2(w,[\alpha\text{Syn}])[\alpha\text{Syn}] \end{cases}$$

$c_t(w)$ is the “threshold concentration”, a linear function of w that defines the position of the inflection point of the sigmoid. The boundary conditions are $[SUV\text{-}\alpha Syn](0) = c_0$, $[\alpha Syn](0) = [\alpha Syn'](0) = 0$. This system of equations, at a first inspection, does not seem to be solvable analytically and attempts to solve it with commercial software for symbolic calculus confirmed this. An attempt to use the fixed point approximation to derive an analytical approximate solution was also made, as it has been recently done in the case of fibrillation kinetics (8), but even after only two iterations of the method the results become too complex to be employed in fitting algorithms for the experimental data. The system was then solved numerically, so that we could compare the time course described by these equations with that obtained from our experiment. Plots of the curves ($[SUV\text{-}\alpha Syn]+[\alpha Syn]$) for $k_1 = 0.6$, $k_2 = 0.1$, $k_3 = 0.1$, $k_4 = 1$, $c_0 = 100$ and $w = 1, 0.5, 0.25$ show a trend very similar to the one observed in the experimental curves. The unfolding gets faster as the dilution factor decreases, the steepness of the sigmoid process increases and the inflection point moves to earlier time points:

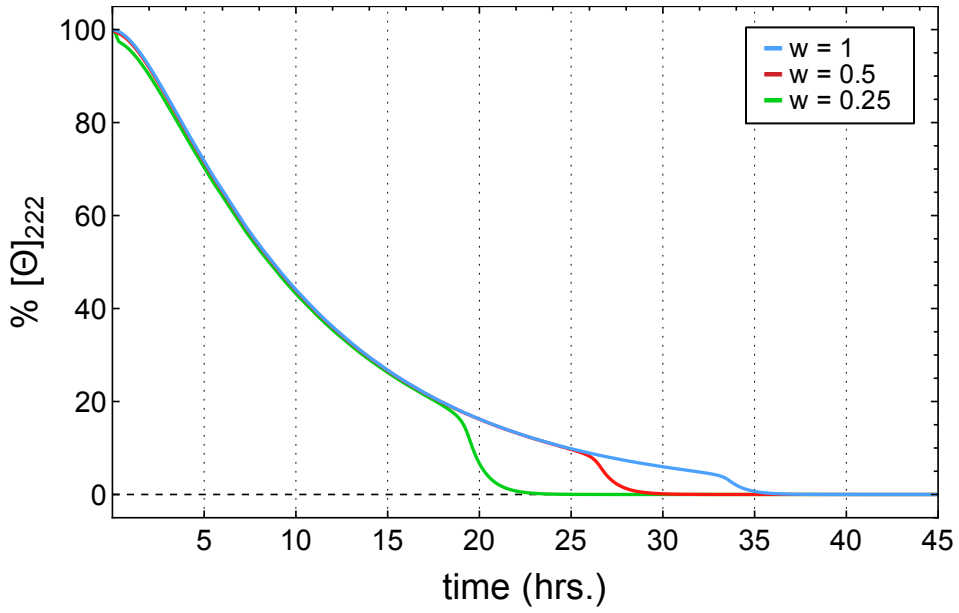

Because of the absence of a reverse lipid-binding process as in **Hp. C**, the shape of the curves in the first part of the exponential (where the sigmoidal term is close to zero) is the same for all three dilutions. The curve for the undiluted sample ($w = 1$) can also be included under the same mechanistic hypothesis since the sigmoid is smooth enough that in the experimental data it could be easily masked by the noise of the signal and the scattering of the vesicles. Given the shape of the curves recorded in the CD-followed unfolding experiments, we can be confident that a cooperative multimerization-like process is present as its effect is clear in the curves with $w = 0.5$ and 0.25, and is consistent with the band pattern of the WB in Fig. S6. Though it was fitted well using a simple exponential decay, the kinetic curve of the undiluted sample, $w = 1$, is almost certainly of the same form, as no change in the unfolding mechanism can be attributed to the dilution of the sample alone and probably just shows a pseudo-exponential decay because of the very shallow shape of its later sigmoid-like phase (Fig. 5B). We can therefore explain the fact that the protein is found to be completely unfolded after SEC (Fig. 4D) with the dramatic dilution of the sample, which leads to the rapid disassembly of metastable multimers according to our kinetic model ($w \approx 0.0125$ under the conditions of the SEC experiment). The alternative interpretation, that αSyn rapidly unfolds due to the removal of the lipid interfaces via SEC is unlikely, given that we could not obtain

experimental evidence for αSyn-lipid interaction above the T_m neither from our kinetic analysis nor from other experimental approaches (see **Hp. C** and Fig. 2).

Mechanistic Hp. C

Since we observed a clear change in the unfolding kinetics of our sample upon dilution and this finding could not be explained by a kinetic description that only involves unimolecular reactions, as in **Hp. A**, another possibility that could be explored involved binding and/or weak association events between αSyn and the SUVs. It must be noted that, while the characterization, by ITC, of the binding process (Fig. 2, Fig. S3B) shows no binding occurring between unfolded αSyn and the SUVs above 10ºC, the equilibria that we are interested in are those of the observed helical αSyn species, which potentially could have a higher affinity for bilayers given the amphipatic nature of the folded helical structures of αSyn previously reported. An addition to the kinetic equations in **Hp. A** was then made, in order to take into account the possibility of a binding/unbinding equilibrium between the binding sites on the SUVs and the folded αSyn conformers (which could explain both the change of the kinetic with the dilutions and the decrease in the lifetime of the folded species with decreasing *w*):

$$[\text{SUV-}\alpha\text{Syn}] \underset{k_3}{\overset{k_1}{\rightleftharpoons}} [\text{SUV}] + [\alpha\text{Syn}] \overset{k_2}{\rightarrow} [\alpha\text{Syn}']$$

$$\begin{cases} \dfrac{\mathrm{d}[\text{SUV-}\alpha\text{Syn}]}{\mathrm{d}t} = -k_1[\text{SUV-}\alpha\text{Syn}] + k_3[\alpha\text{Syn}](c_0 - [\alpha\text{Syn}]) \\ \dfrac{\mathrm{d}[\alpha\text{Syn}]}{\mathrm{d}t} = k_1[\text{SUV-}\alpha\text{Syn}] - k_3[\alpha\text{Syn}](c_0 - [\alpha\text{Syn}]) - k_2[\alpha\text{Syn}] \\ \dfrac{\mathrm{d}[\alpha\text{Syn}']}{\mathrm{d}t} = k_2[\alpha\text{Syn}] \end{cases}$$

The boundary conditions are *[SUV-αSyn](0) = c_0*, *[αSyn](0) = [αSyn'](0) = 0*. Again, this system of ODEs has no analytical solution (and the fixed-point method leads to equally intractable expressions as in the previous case) so numeric solutions were calculated for the three dilution factors. Plots of the curves (again of *[SUV-αSyn]+[αSyn]*) for k_1 = 0.15, k_2 = 0.7, k_3 = 0.6, c_0 = 100 and *w* = 1, 0.5, 0.25 confirm the qualitative assessment of the time course:

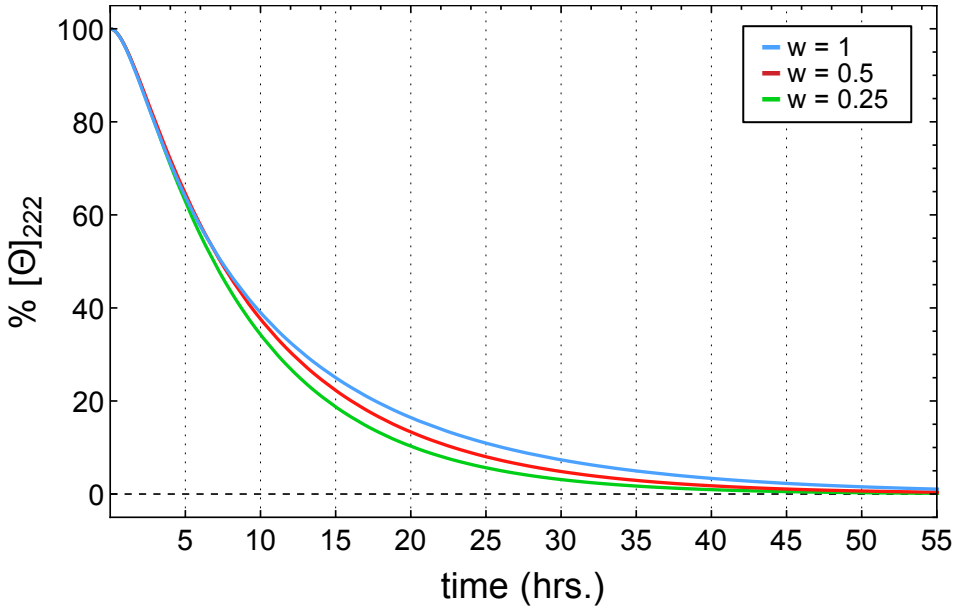

The shape of the curves changes with *w* and the lifetime of the folded species decreases with the decrease in *w* (as the rate of the reverse reaction *[SUV][αSyn]* → *[SUV-αSyn]* decreases). Even if this addition describes some of the trends observed experimentally, it cannot be considered an optimal model for the complex, biphasic, shape of the kinetic curves at *w* = 0.5 and 0.25 (Fig. 4). In addition to that, in our unfolding curves we do not observe the concentration dependence at early times that this model would predict. It has to be noted, however, that the lipid-rebinding process, given the small magnitude of its effect on the kinetics, could be masked by the noise of the CD signal (S/N ratio decreases as the signal decreases, i.e. with the decrease in *w*) or the scattering signal of the SUVs. We concluded that intermittent lipid-binding alone, even though it follows some of the observed trends in kinetic constants, cannot entirely explain our observations.

SI References

1. Johnson M, Coulton AT, Geeves MA., Mulvihill DP (2010) Targeted amino-terminal acetylation of recombinant proteins in E. coli. *PLoS One* 5(12):e15801.
2. DeTure M, et al. (2000) Missense tau mutations identified in FTDP-17 have a small effect on tau-microtubule interactions. *Brain Res* 853(1):5–14.
3. Dettmer U, Newman AJ, Luth ES, Bartels T, Selkoe D (2013) In vivo cross-linking reveals principally oligomeric forms of α-synuclein and β-synuclein in neurons and non-neural cells. *J Biol Chem* 288(9):6371–85.
4. Chen PS, Toribara TY, Huber W (1956) Microdetermination of Phosphorus. *Anal Chem* 28(11):1756–1758.
5. Cantor CR, Schimmel PR (1980) *Biophysical Chemistry. Part III: The Behavior of Biological Macromolecules* (W.H.Freeman & C., New York).
6. House JE (2002) *Principles of chemical kinetics* (Academic Press, Burlington, MA). 2nd Ed.
7. Bartels T, Choi JG, Selkoe DJ (2011) α-Synuclein occurs physiologically as a helically folded tetramer that resists aggregation. *Nature* 477(7362):107–10.
8. Knowles TPJ, et al. (2009) An analytical solution to the kinetics of breakable filament assembly. *Science* 326(5959):1533–7.

SI Figures

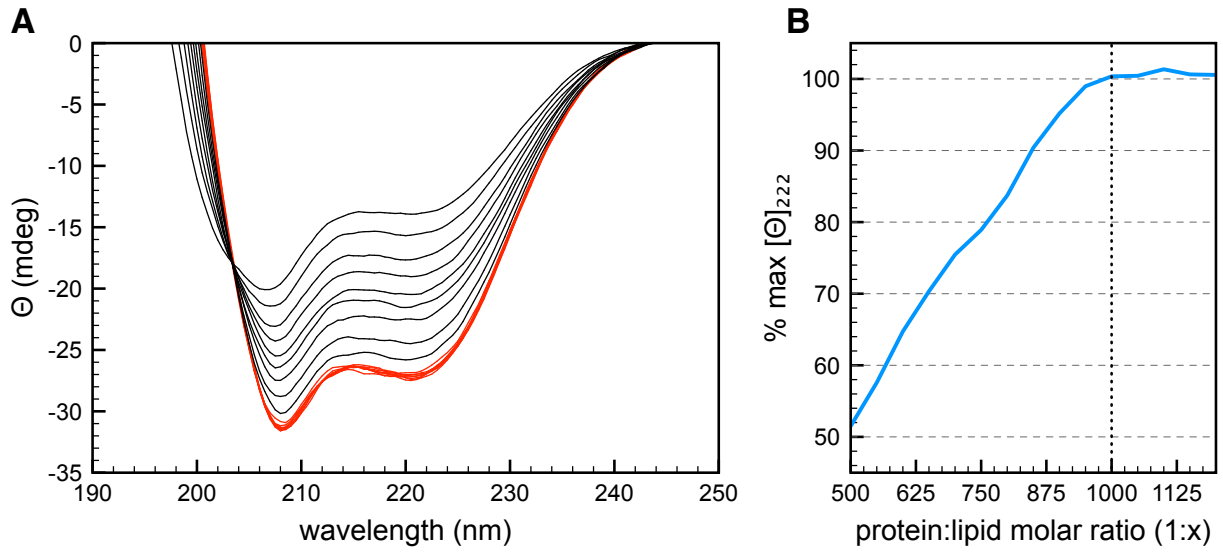

Fig. S1. (A) Circular dichroism (CD) spectra of samples of αSyn titrated with 13:0 PC SUVs, measured at 25ºC (corrected for the dilution from the addition of titrant). The spectra shown in (A) have a protein:lipid molar ratio ranging from 1:500 to 1:1250. The spectra in red (1:1000 - 1:1250) correspond to the endpoint of the titration. (B) Percentage of the maximum 222-nm molar ellipticity signal (the plateau value of the titration has been set at 100%) of αSyn titrated with 13:0 PC SUVs and measured at 25ºC, plotted against the corresponding protein:lipid molar ratio. The dotted line at (protein: lipid molar ratio) 1:1000 marks the endpoint of the titration.

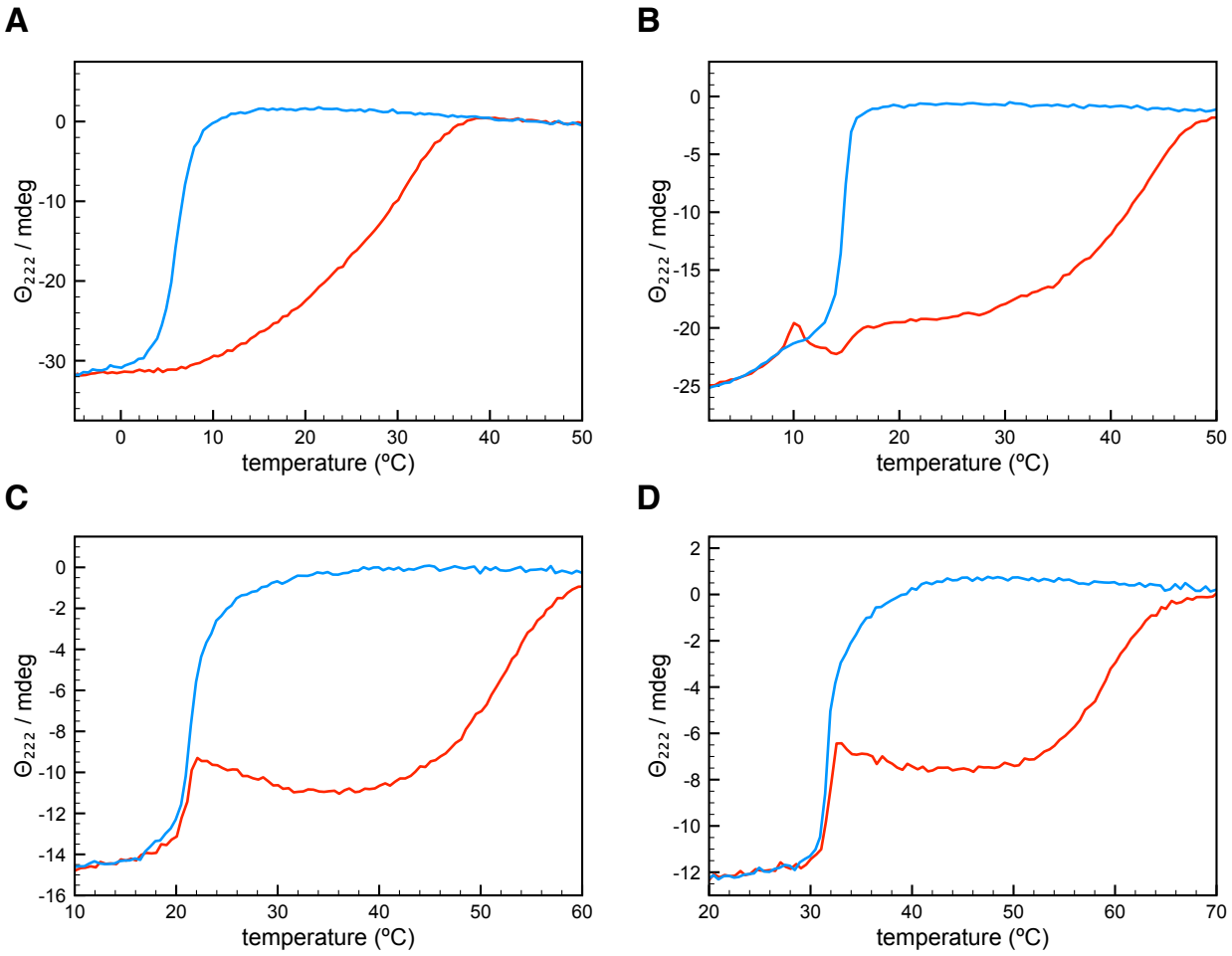

Fig. S2. Ellipticity signal at 222 nm of 5 μM αSyn refolded in the presence of (A) 5 mM 12:0 PC SUVs, (B) 5 mM 13:0 PC SUVs, (C) 5 mM 14:0 PC SUVs and (D) 5 mM 15:0 PC SUVs through temperature scans, followed by circular dichroism (CD), recording the signal every 0.5ºC and using a 0.5ºC/min. gradient. Blue curves indicate downscans, red curves indicate upscans.

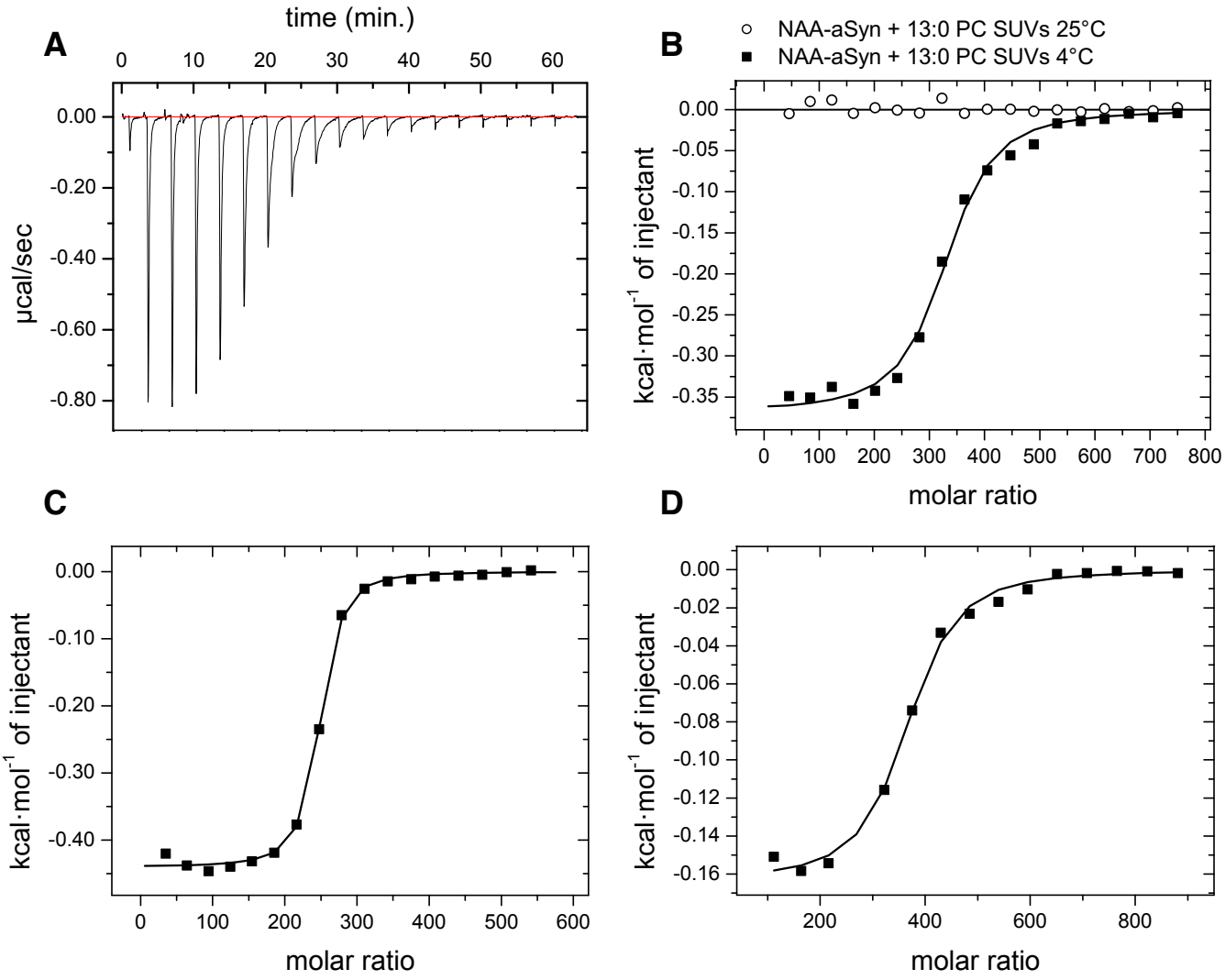

E

	N	K_{app}	$N \cdot K_{app}$	ΔH *(cal/mol)*	ΔS *(cal/mol·K)*
13:0 PC (4ºC)	$(3.17\pm0.04)\cdot10^{2}$	$(3.3\pm0.6)\cdot10^{4}$	$\mathbf{(1.0\pm0.2)\cdot10^{7}}$	-368±7	19.3
14:0 PC (4ºC)	$(2.35\pm0.01)\cdot10^{2}$	$(2.4\pm0.3)\cdot10^{5}$	$\mathbf{(5.6\pm0.7)\cdot10^{7}}$	-440±3	23.0
15:0 PC (4ºC)	$(3.48\pm0.04)\cdot10^{2}$	$(3.2\pm0.5)\cdot10^{4}$	$\mathbf{(1.1\pm0.2)\cdot10^{7}}$	-163±3	20.0

Fig. S3. Isothermal titration calorimetry (ITC) representative differential heat signal (A) and binding curves of 5µM αSyn titrated with freshly prepared (B) 13:0 PC SUVs (both at 4ºC and 25ºC), (C) 14:0 PC SUVs (at 4ºC) and (D) 15:0 PC SUVs (at 4ºC) plotted along with their fitting function curves (solid lines). No binding process was detected between αSyn and 13:0 PC SUVs at 25ºC. (E) Thermodynamic and stoichiometric parameters obtained from the fitting of the binding curves with an N-independent binding sites model, with standard errors.

	DLS-measured radius (nm)
12:0 PC SUVs	**21.7±0.7**
13:0 PC SUVs	**19.2±0.5**
14:0 PC SUVs	**25±3**
15:0 PC SUVs	**38±5**

Supporting Table 1. Mean radii of freshly prepared suspensions of 12:0, 13:0, 14:0 and 15:0 PC SUVs (along with SDs obtained from 3 independent samples), measured via DLS.

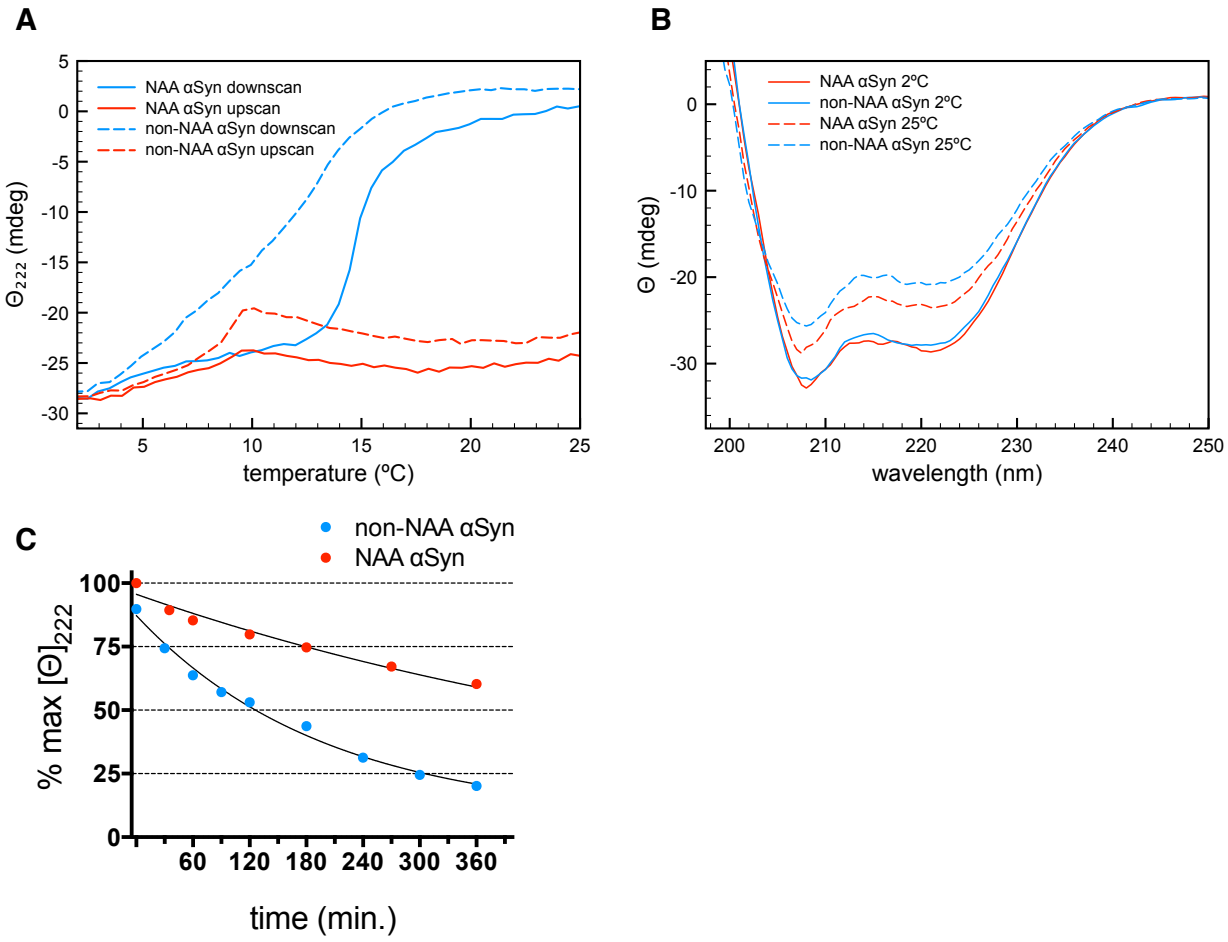

Fig. S4. (A) Ellipticity signal at 222 nm of 10 μM N-alpha-acetylated (NAA)/non-NAA αSyn refolded in the presence of 12 mM 13:0 PC SUVs via temperature cycling followed by circular dichroism (CD), recording the signal every 0.5ºC and using a 0.5ºC/min. gradient. Blue curves indicate downscans, red curves indicate upscans. (B) Circular dichroism spectra of samples of NAA/non-NAA αSyn refolded via temperature cycling in the presence of 13:0 PC SUVs, measured at 25ºC. The CD spectra of the samples at the lower end of the temperature scan (2ºC) are shown for comparison. (C) Percentage of the 222-nm molar ellipticity signal (100% for NAA-aSyn at 0h) of NAA/non-NAA αSyn refolded via temperature cycling in the presence of 13:0 PC SUVs and measured at 25ºC over 6 hrs (measured from the end of the temperature scan). The data were fitted with exponential curves (shown in black), with % $[\Theta]_{222}(0)$ and the decay time (τ) as free parameters and with the plateau value as a global parameter shared by both datasets.

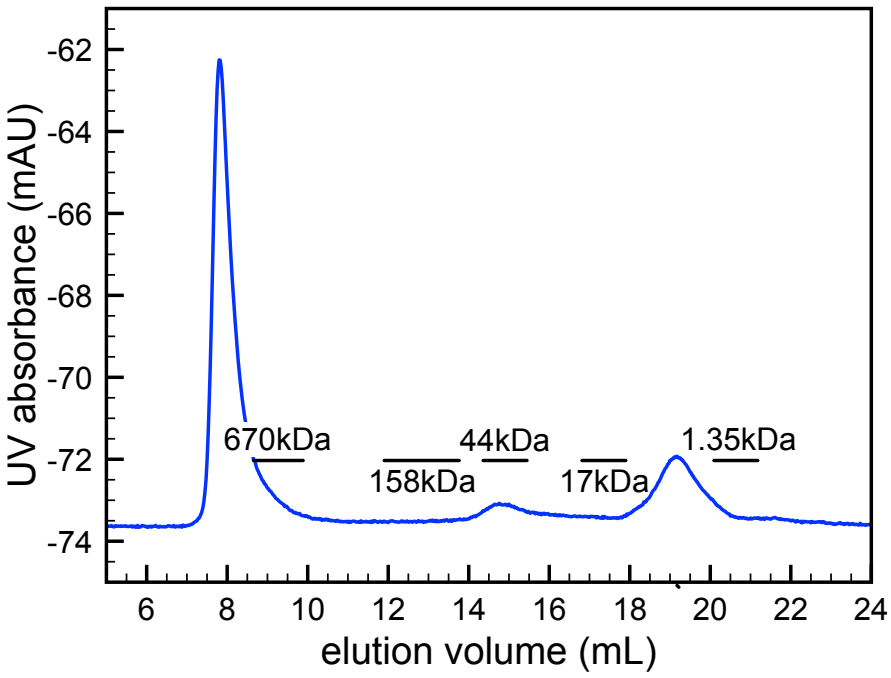

Fig. S5. Size-exclusion chromatography (SEC) chromatogram of a sample of αSyn refolded via temperature cycling in the presence of 13:0 PC SUVs. The blue trace shows the absorbance at 280 nm. Black lines indicate the approximate peak widths of the SEC standards run on the column, along with their molecular weights. 1-mL fractions were collected between 6 mL and 24 mL.

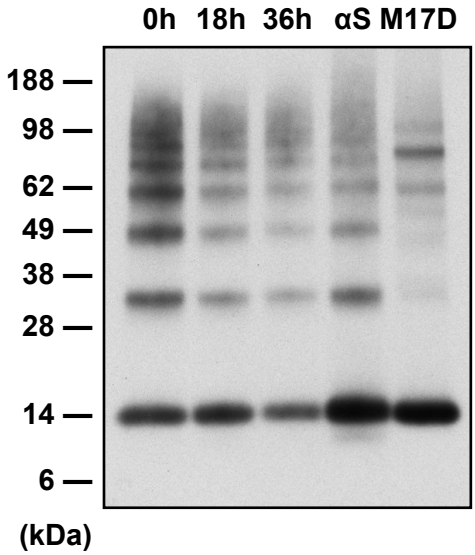

Fig. S6. Western-blot of the cross-linking reactions performed using 500 μM disuccinimidyl glutarate (DSG) on the supernatant fraction of αSyn refolded via temperature cycling in the presence of 13:0 PC SUVs. Samples were taken from the supernatant, incubated at RT, and cross-linked 0, 18 or 36 hrs after the end of the ultracentrifuge spin *(0h, 18h, 36h)*. Samples of intact αSyn-overexpressing M17D cells cross-linked with 1 mM DSG, *(M17D)* and of 7.5μM recombinant αSyn cross-linked with 500μM DSG, *(αS)* are shown for comparison.

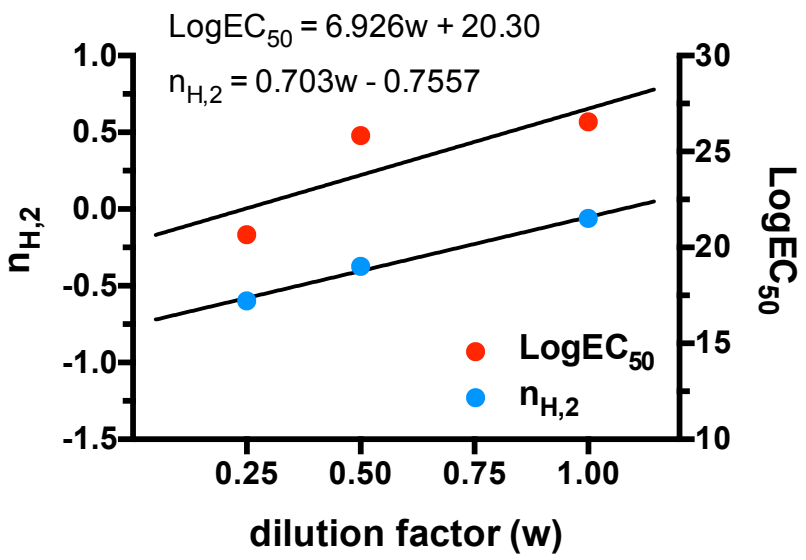

Fig. S7. Plot of the fitting parameters for the CD-followed unfolding data at different dilution factors (Fig. 5) vs. the dilution factor *w* for the corresponding curve. A biphasic (double-sigmoid) model was used to qualitatively fit the data, keeping all the parameters equal while varying *w*, except for the cooperativity (steepness) of the second sigmoid, $n_{H,2}$, and the inflection point of the same transition, $LogEC_{50,2}$. Linear regression curves are also plotted for the two parameters, and their equations are shown in the graph.